# Effect of surface treatment on an n-CdSe0.6Te0.4 thin-film photoanode/polysulphide electrolyte solar cell

V. Damodara Das and Laxmikant Damodare

Citation: Journal of Applied Physics **81**, 1522 (1997); doi: 10.1063/1.363913
View online: http://dx.doi.org/10.1063/1.363913
View Table of Contents: http://scitation.aip.org/content/aip/journal/jap/81/3?ver=pdfcov
Published by the AIP Publishing

# Effect of surface treatment on an $n$-$CdSe_{0.6}Te_{0.4}$ thin-film photoanode/polysulphide electrolyte solar cell

V. Damodara Das[a] and Laxmikant Damodare
*Thin Film Laboratory, Department of Physics, Indian Institute Technology, Madras, Madras 600 036, India*

(Received 20 May 1996; accepted for publication 30 September 1996)

Polycrystalline thin films of $n$-$CdSe_{0.6}Te_{0.4}$ were deposited in a vacuum of $5\times10^{-5}$ Torr by thermal flash evaporation with a deposition rate of $20\pm1$ Å/s on indium oxide coated glass plates [$\sigma=1.25\times10^{4}$ $(\Omega\ \mathrm{cm})^{-1}$] held at 200 °C. Application of surface treatment techniques such as annealing and photoelectrochemical etching on the films revealed that the films exhibit photoelectrochemical behavior with increased conversion efficiency and stability after treatment. Gärtner's model [Phys. Rev. **116**, 84 (1954)] was used in the calculation of the solid state parameters of the films like the carrier concentration $N_D$ and minority carrier diffusion length $L_p$ for different surface treatments. Chemical etching improves the efficiency and fill factor from 1.53% and 40% to 2.72% and 50% respectively, whereas photoelectrochemical etching improves further the efficiency to 3.83% and fill factor to 59% and the stability of the photoelectrode in the polysulphide electrolyte. © *1997 American Institute of Physics.* [S0021-8979(97)05001-9]

## I. INTRODUCTION

For a photoelectrochemical solar cell, the prime requirement for good solar energy conversion is that the photocathode/photoanode should have a band gap close to the maximum in the visible spectrum to utilize the solar spectrum efficiently; second the semiconductor electrodes must be stable against photocathodic/photoanodic reactions.[1,2] Presently, one of the best materials where tailoring of band gap is possible is from the group of *Cd*-chalcogenides,[3,4] viz., $n$-$CdSe_{0.6}Te_{0.4}$ which has a band gap very close to the maximum in the visible spectrum, $\approx1.45$ eV. However, very low effciency of the photoelectrochemical cells can be attributed to the loss of photogenerated carriers due to the recombination at the grain boundaries in polycrystalline thin films. In order to optimize the performance of the photoelectrochemical cell, we have carried out investigations on the influence in solar energy conversion of etching, photoelectrochemical etching, and annealing on the performance of an $n$-$CdSe_{0.6}Te_{0.4}$ thin-film photoelectrode.

## II. EXPERIMENTAL DETAILS

### A. Preparation of $n$-$CdSe_{0.6}Te_{0.4}$ alloy

Measured quantities of high purity (99.999%) constituent elements, viz., Cd, Se, and Te (obtained from Nuclear Fuel Complex, Department of Atomic Energy, Government of India, Hyderabad, India) were taken in a precleaned quartz ampoule of 15 mm diameter and 150 mm length and evacuated to $5\times10^{-5}$ Torr and then vacuum sealed. The ampoule was initially kept at 220 °C for about 10 h and then heated slowly to the melting point of the alloy. By means of a digitally controlled temperature controller attached to the furnace, the temperature of the ampoule was kept stable at 950 °C for about 1 day. The resulting alloy was annealed in vacuum at 950 °C for 1 h and then subjected to controlled cooling at the rate of 25 °C/h to room temperature. The bulk alloy thus prepared by the above technique was finely powdered using an agate mortar and pestle.

### B. Thermal flash evaporation of $n$-$CdSe_{0.6}Te_{0.4}$ alloy

$n$-$CdSe_{0.6}Te_{0.4}$ alloy thin films of thickness $\approx4000$ Å were deposited by thermal flash evaporation of finely powdered $n$-$CdSe_{0.6}Te_{0.4}$ alloy in a vacuum of $5\times10^{-5}$ Torr on indium oxide thin film precoated glass substrates held at 200 °C. The method of preparation of indium oxide thin films is reported elsewhere by the authors.[5] Annealing of the as-grown films was carried out at a constant temperature of $300\pm5$ °C in air for 1 h and utmost care was taken not to exceed the temperature of the thin films to such an extent that the distortion of the flatness of the glass plates took place due to the proximity of the glass melting point. Optical absorption studies were performed on $n$-$CdSe_{0.6}Te_{0.4}$ thin films grown on bare glass plates by means of a Hitachi recording spectrophotometer (Model U3400) in the UV–visible–near infrared (UV-VIS-NIR) range. The contribution of the bare glass plate to the optical absorption (even though small) was subtracted from the total optical absorption of the thin film and glass plate combination to get the net optical absorption in calculating the values of the optical-absorption coefficient for each wavelength. X-ray diffraction (XRD) patterns were recorded with the help of a Philips x-ray machine using Cu $K\alpha$ x-ray radiation.

### C. Fabrication of photoelectrochemical solar cell

Photoelectrochemical solar cell was fabricated using the as-grown $n$-$CdSe_{0.6}Te_{0.4}$ thin film as the photoanode. A three-electrode configuration, comprising $n$-$CdSe_{0.6}Te_{0.4}$ thin-film photoanode, graphite as a counter electrode, and a saturated calomel electrode (SCE) as a reference electrode, was used for measurements in the dark. Redox electrolyte used was aqueous 1 M $Na_2S$+1 M NaOH+1 M S. All the reagents and chemicals used were of analytical reagent (AR) grade. The photoanode area exposed to light was

[a]Electronic mail: vddas@acer.iitm.ernet.in

 0021-8979/97/81(3)/1522/9/$10.00 

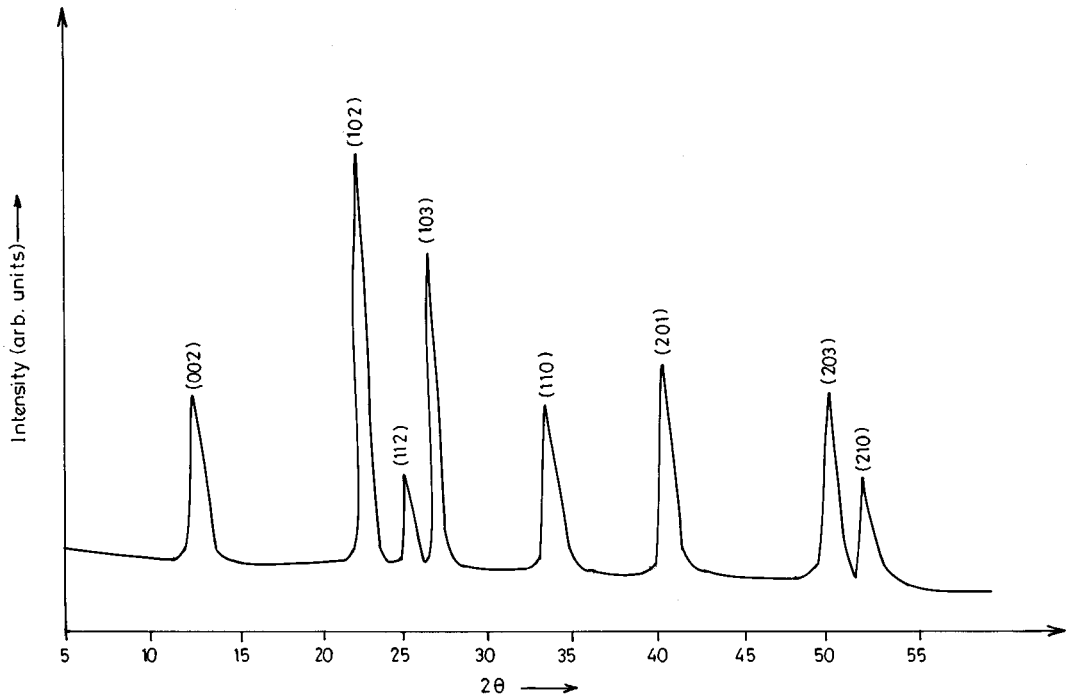


FIG. 1. An x-ray diffractogram of a typical $n$-$CdSe_{0.6}Te_{0.4}$ thin film.

$(2.75\times1.75) \approx 4.1\ cm^2$. A photoelectrochemical solar cell was achieved by dipping the film in the above redox electrolyte in an airtight setup to avoid interaction of oxygen with the redox electrolyte. The area of the semiconducting thin film other than that in contact with the electrolyte was covered by epoxy resin (Araldite, made in India) to annull any contribution due to the contact of the base contact oxide material with the electrolyte and its interference in the measured value of the net photocurrent density.

For measurements of power output characteristics, a two-electrode configuration consisting of the thin-film photoanode and graphite as the counter electrode was used. All current and voltage measurements were made by using Keithley (Cleveland, OH) (model 175) Digital automultimeters. Measurements for the power output characteristics, Mott–Shottky ($C-V$) plots, and current–voltage plots were not made by the conventional continuous sweep method but were made at fixed intervals after waiting long enough for the system to equlibriate at that setting (both in the dark as well as under illumination). While the measurements were in progress, no stirring of the electrolyte was done. However, the electrolyte was purged with AR grade argon gas before the commencement of measurements to remove the embedded oxygen in the electrolyte during its preparation. No purging with argon gas was done once the experiments commenced. Capacitance–voltage measurements were carried out in the dark at a frequency of 1 kHz. The amplitude of the sinusoidal ac signal was kept constant at a 10 mV peak-to-peak value and $C-V$ data were collected and Mott–Schottky plots were drawn for the $n$-$CdSe_{0.6}Te_{0.4}$ thin-film/polysulphide junction. In all cases, large area ohmic contacts of high-purity indium (99.999% purity) were made to the base substrate indium oxide thin film by vacuum deposition to minimize the series resistance of the solar cell and they were covered by the epoxy resin to avoid any photoeffects on illumination at the contacts.

Etching of thin films was carried out in the dark for 10 s in a solution of 3 ml HCl+1 ml $HNO_3$+25 ml $H_2O$. Films were thoroughly washed in flowing de-ionized ($\rho\approx15$ M $\Omega$ cm) doubly distilled water before subjection to photoelectrochemical measurements. Photoelectrochemical etching was done in a freshly prepared solution of the same composition as mentioned above but by illuminating the photoelectrode thin film by white light illumination of intensity 100 mW/cm$^2$ using a tungsten filament-halogen lamp of rating 250 V/500 W without any bias from external battery power source for 10 s by shorting the photoelectrode and the counter electrode (graphite). Mott–Schottky plots were drawn by collecting $C-V$ data (using a RADART *LCR* bridge) at a frequency of 1 kHz. Surface analysis was done using a JEOL JXA-840 scanning electron microscope (SEM) used for surface morphology studies with working voltage of 20 kV and a constant probe current of $3\times10^{-10}$ A. Prior to SEM analysis all the specimens were sputter-coated with a 70 Å thin film of gold to enhance their electrical conductivity.

## III. RESULTS AND DISCUSSION

### A. X-ray diffraction studies

As-grown films were characterized by XRD using Cu $K\alpha$ radiation with a Ni filter. The XRD pattern obtained (Fig. 1) for the film grown on bare microslide glass plates was studied in the $2\theta$ range 5°–60°. The XRD pattern showed that the films were microcrystalline (polycrystalline). From the $d$ values obtained (Table I) it was concluded that

TABLE I. Comparison of observed $d$ values from x-ray-diffraction pattern with the values from literature for a typical $n$-$CdSe_{0.6}Te_{0.4}$ film.

| Serial number | $d^a$ (Å) | $d^b$ (Å) | $h\ k\ l$ |
|---|---|---|---|
| 1 | 1.758 | 1.743 | 2 1 0 |
| 2 | 1.823 | 1.816 | 2 0 3 |
| 3 | 2.253 | 2.246 | 2 0 1 |
| 4 | 2.599 | 2.593 | 1 1 0 |
| 5 | 3.349 | 3.352 | 1 0 3 |
| 6 | 3.560 | 3.588 | 1 1 2 |
| 7 | 3.949 | 3.967 | 1 0 2 |
| 8 | 7.078 | 7.089 | 0 0 2 |

[a]Observed.
[b]From Refs. 6–9.

the films exhibit hexagonal symmetry with $a_0=6.3$ Å and $c_0=11.3$ Å. The presence of a homogeneous hexagonal phase is consistent with the observations of other workers.[6]

### B. Optical-absorption studies

Optical absorption studies were carried out on $n$-$CdSe_{0.6}Te_{0.4}$ films deposited on bare precleaned glass plates in the wavelength range 300–900 nm at room temperature. For allowed direct band-gap electronic transitions, the absorption coefficient $\alpha$, near the absorption edge, is given by[10]

$$\alpha \approx \frac{A}{h\nu}(h\nu - E_g)^{1/2}, \tag{1}$$

where $h$ is Planck's constant, $\nu$ is the frequency of the incident light, and the coefficient $A^*$ is given by

$$A^* \approx q^2\left(\frac{2m_e^* m_h^*}{m_e^* + m_h^*}\right)(nch^2 m_e^*)^{-1}, \tag{2}$$

where $m_e^*$ and $m_h^*$ are the electron and hole effective masses respectively, $c$ is the speed of light, $q$ is the electron charge, and $n$ is the refractive index. Hence, if $(\alpha h\nu)^2$ is plotted against h$\nu$, the plot will be a straight line according to Eq. (1). The experimental plot of $(\alpha h\nu)^2$ vs $h\nu$ is found to be linear (Fig. 2) indicating that the nature of the band gap of semiconducting $n$-$CdSe_{0.6}Te_{0.4}$ is direct. The intercept on the energy axis at $\alpha=0$ yields $E_g \approx 1.45$ eV which agrees well with the band-gap value given by other authors.[11]

### C. Photoelectrochemical characterization of thin films

#### 1. Mott–Schottky plot analysis

Substituting the expression for the depletion layer width in the semiconductor $\omega$ in the expression for the space-charge capacitance $C_s$, of the space-charge layer formed due to the semiconductor-electrolyte junction formation, we get the Mott–Schottky[12,13] relation

$$1/C_{sc}^2 = \frac{2}{q\epsilon_0\epsilon_s N_D A^2}\left(V - V_{FB} - \frac{k_B T}{q}\right), \tag{3}$$

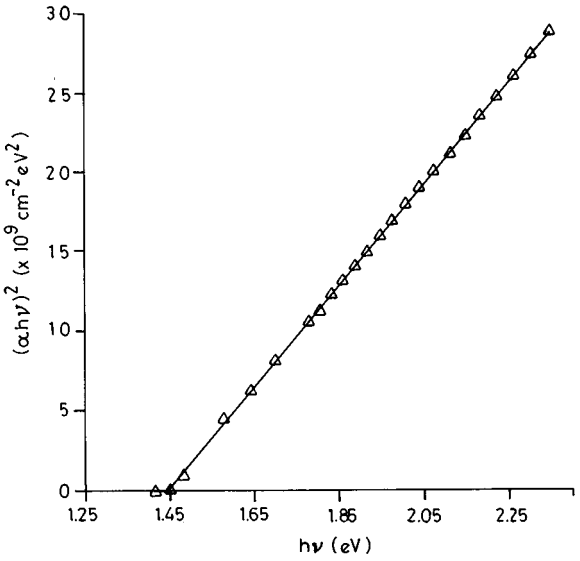


FIG. 2. $(\alpha h\nu)^2$ vs $h\nu$ plot of $n$-$CdSe_{0.6}Te_{0.4}$ thin film of thickness 4000 Å.

where $q$ is the electronic charge, $k_B$ is the Boltzmann constant, $T$ is the absolute temperature, $V$ is the electrode potential, $V_{FB}$ is the flatband potential, and $N_D$ is the majority carrier charge density.

The value of the electrode potential at $1/C_{sc}^2 = 0$ gives the flatband potential and the slope of the plot gives the majority carrier charge density $N_D$ in the space-charge region.

Figure 3 shows the Mott–Schottky plots obtained for the unannealed and annealed films, respectively, at 1 kHz frequency. It can be seen that on annealing the thin films there is a slight change in the slope of the Mott–Schottky plot. The donor concentration obtained from these Mott–Schottky plots increases from $3.98\times10^{17}$ to $6.15\times10^{17}$ cm$^{-3}$, respec-

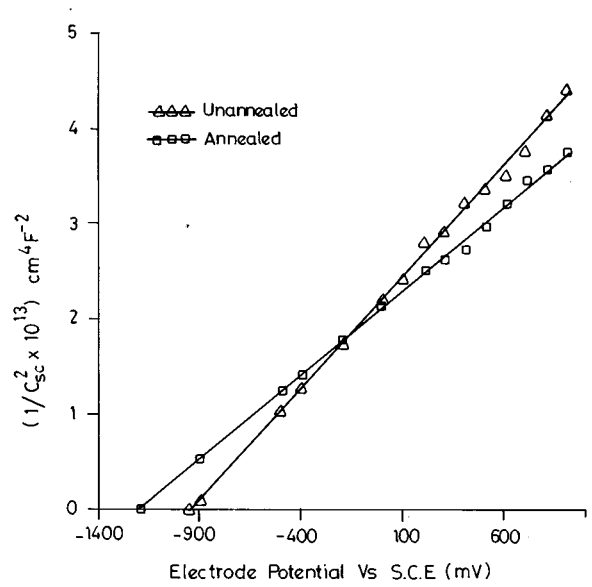


FIG. 3. Mott–Schottky plots for the annealed and unannealed $n$-$CdSe_{0.6}Te_{0.4}$/polysulphide system.

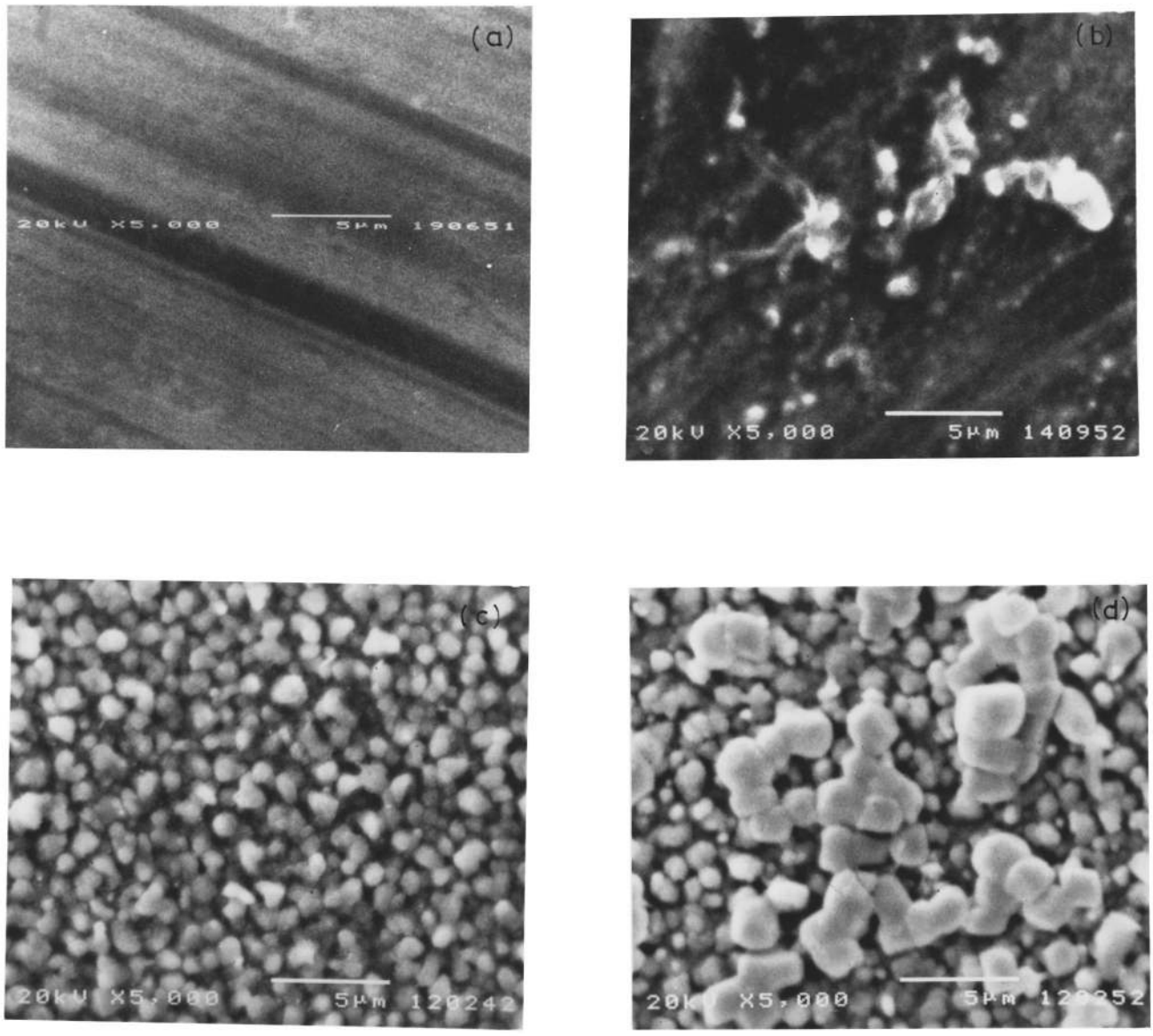


FIG. 4. Scanning electron micrographs of (a) as-grown film, (b) etched film, (c) annealed film, (d) PEC etched film (magnification: 500×20 kV).

tively. This is due to the fact that upon annealing there is an increase in the grain size and, hence, an increase in the minority carrier diffusion length and concurrent decrease in the scattering by the grain boundaries. Figure 4(a) shows the (SEM) of the as-grown film. Figure 4(b) shows the SEM micrograph of the etched film, Fig. 4(c) shows the SEM micrograph of the annealed and etched film, and Fig. 4(d) shows the SEM micrograph of the annealed and photoelectrochemically etched film. Increase in grain size due to annealing and agglomeration of grains due to etching can be seen in the above figures. Grain size is determined from the intercept method,[14,15]

$$\text{grain size} = 1.5 \times l/(nm), \tag{4}$$

where $m$ is the micrograph magnification, $l$ is the line length on the micrograph, $n$ is the number of grains crossed by the line, and 1.5 is the parameter assuming spherical grains.[15]

The grain size as determined from the intercept method increases from 12 to 2000 Å and the grain density decreases from $1.38\times10^{20}$ to $2.98\times10^{13}$ $\text{cm}^{-3}$. In the annealed and photoelectrochemically etched films, the grain size is ≈6000 Å and the grain density is $4.42\times10^{12}$ $\text{cm}^{-3}$.

Annealing promotes fusion of small crystallites (agglomeration), thus reducing the grain-boundary area, which leads to the increase in diffusion length due to the decrease in scattering from the boundaries. Also, annealing removes excess Cd, so that recombination centers such as Cd acceptors are also removed. It should be noted here that the donor concentrations obtained from these plots are the donor concentrations near the film surface in the depletion region only and not the average value of the bulk of the film.

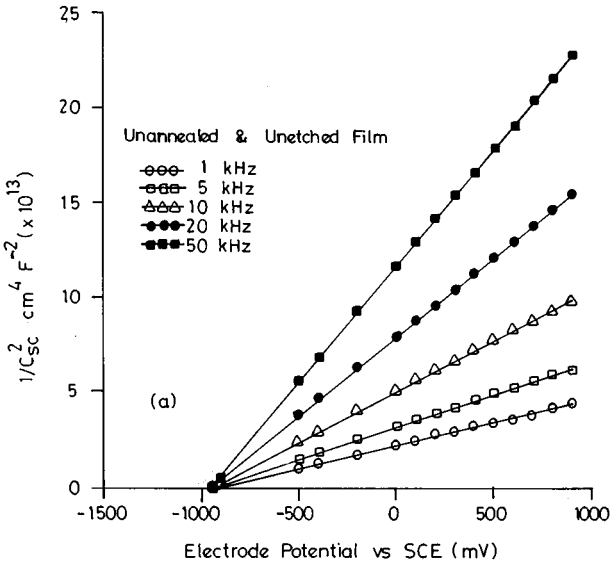


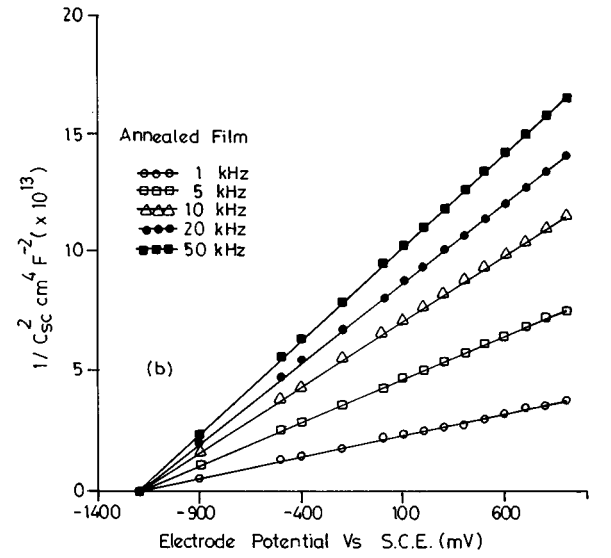


FIG. 5. (a) Mott-Schottky plots for the unannealed film used for $n$-$CdSe_{0.6}Te_{0.4}$ /polysulphide system at frequencies of 1, 5, 10, 20, and 50 kHz. (b) Mott–Schottky plots for the annealed film used for $n$-$CdSe_{0.6}Te_{0.4}$/polysulphide system at frequencies of 1, 5, 10, 20, and 50 kHz.

### 2. Frequency dispersion of Mott–Schottky plots

Figure 5(a) shows the Mott–Schottky plots drawn for the as-grown film for the PEC characterization. It is seen that there is a large dispersion in the Mott–Schottky plots. The slope of the plots also increases with frequency in the range 1–50 kHz. It is seen that the plots converge at a single point on the $x$ axis, as also observed by the authors[16] and other workers.[17–21]

Contribution to frequency dispersion can be due to the bulk property of the space-charge layer and occurence of most of the applied voltage over the Helmholtz layer.[18] It can also be due to:[17]

(a) a small contribution from the bulk of the electrode, back oxide ohmic contact, and impedance during the measurements;

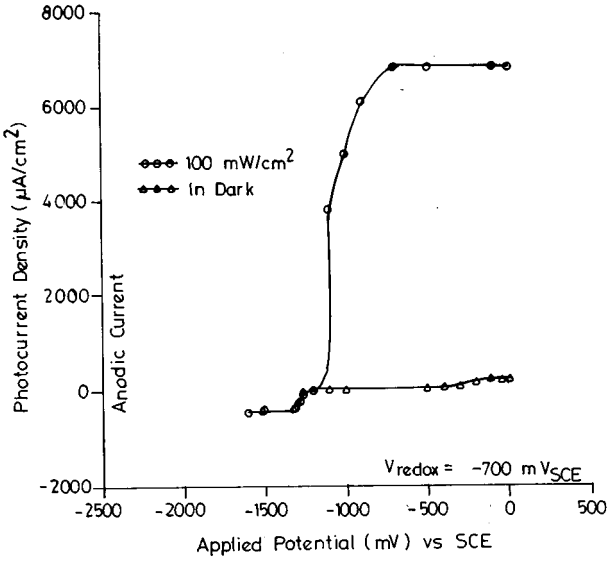


FIG. 6. Typical photocurrent density vs applied potential plot of $n$-$CdSe_{0.6}Te_{0.4}$/polysulphide PEC solar cell. Bottom curve signifies a feeble cathodic dark current.

(b) irregular surface of the film leading to uneven distribution of the modulated input ac signal;
(c) small contribution of surface states to capacitance;[18]
(d) some amount of surface roughness of the semiconducting thin film electrode; and
(e) non-uniform distribution of donor species in the region close to the surface of the semiconductor.

Figure 5(b) indicates that the annealing of the thin film leads to some change in the plots; however, dispersion persists even though the change in the slope is less than that in the as-grown unannealed films. This can be explained by the fact that the annealed film has large grains and less grain-boundary area due to annealing, so that irregularities are removed to some extent leading to the reduction in the surface states at the semiconductor–electrolyte boundary. Also, the response of impurities trapped at the grain boundaries contributes to an increase in the slope and dispersion in the plots.

Annealing enhances the structural rearrangement of the donor atoms in the film and annealing-*cum*-PEC etching of the film leads to the removal of partial contribution of surface states to some extent but the plots do not exhibit remarkable change from those of the annealed films. Annealing of the film leads to the near-uniform distribution of donor concentration in the near proximity of the surface of the film, leading to the decrease in the slope.

### 3. Current–voltage characteristics

Figure 6 shows the photocurrent density versus applied potential plot for the as-grown thin-film PEC cell. It is seen from the plot that there is a shift of current on illumination toward the positive side, indicating that the current is an anodic current, which indicates that the semiconducting film

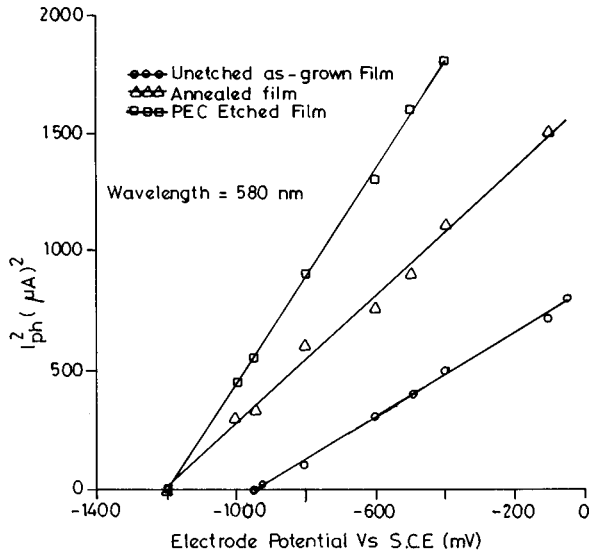


FIG. 7. A plot of $I_{ph}^2$ vs Electrode potential for a monochromatic wavelength of 580 nm for the as-grown, annealed film and annealed-*cum*-PEC etched film.

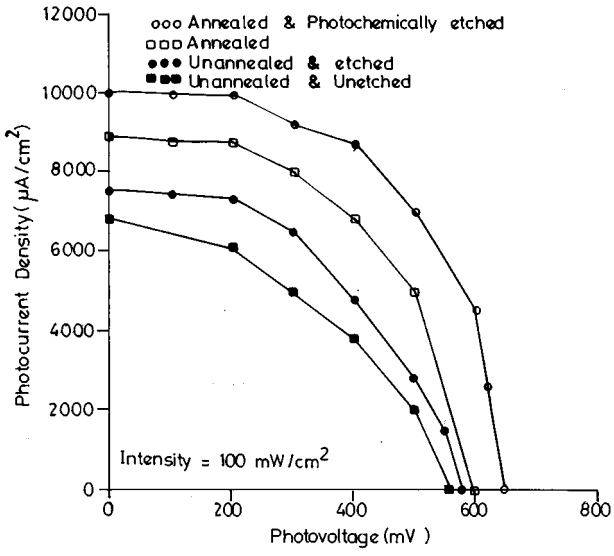


FIG. 8. Plot of power output characteristics for a typical $n$-$CdSe_{0.6}Te_{0.4}$/polysulphide PEC solar cell.

is $n$ type[22] and the photoelectrode on illumination behaves as a photoanode. The value of the flatband voltage, $V_{FB}$ (vs SCE) can be measured from[23]

(i) the onset potential of photocurrent of $J-V$ characteristics under illumination, and

(ii) the voltage intercept of the Mott–Schottky plot. The onset of photocurrent at a potential gives the value of the flatband voltage $V_{FB}$ of $\approx -1200$ mV versus SCE. The reason for this is that at the flatband potential there is no current flow due to the absence of any field across the space-charge layer which can separate the charge carriers. Thus, an externally applied potential slightly more than the flatband voltage can create a field across the space-charge layer that can affect the separation of photogenerated charges leading to the onset of photocurrent in the external circuit. That potential is the flatband voltage, which is quite close to the value measured from the Mott–Schottky plot, $\approx -1205$ mV versus SCE.

(iii) According to Butler,[24] for $\alpha\ L_p \ll 1$ the relation between the applied potential and the photocurrent for monochromatic incident light is given by

$$V - V_{FB} \approx [I_{ph}/(\alpha A \omega_0 q \phi_0)]^2. \tag{5}$$

The experimental plot of $I_{ph}^2$ versus applied potential for a wavelength of 580 nm is linear (Fig. 7) with an intercept of $\approx -1220$ mV versus SCE (i.e., as the flatband voltage). The expression of $\omega_0$ is given by[24,25]

$$\omega_o = [2\epsilon_s \epsilon_o/(qN_D)]^{1/2}. \tag{6}$$

Equation (5) can be further simplified using the expression for $\omega_0$ as[24]

$$V - V_{FB} \approx [N_D/(2\epsilon_o \epsilon_s q)][I_{ph}/(\alpha A \phi_o)]^2. \tag{7}$$

It is seen that the $N_D$ values calculated from the above expression decrease from $1.9\times10^{17}$ to $0.7\times10^{17}$ cm$^{-3}$ for the annealed, unetched film to PEC etched film; hence the calcualted average values obtained for $N_D$ from the plot of $I_{ph}^2$ versus applied voltage show a decreasing trend upon surface treatment. The $N_D$ values determined by the photocurrent data refer to the average donor concentration of the whole bulk film. The values of $N_D$ calculated from the Mott–Schottky plots refer to the depletion region near the semiconductor–electrolyte junction. Thus, there is necessarily a change in the values of $N_D$ obtained by the two methods and also in the trend.

Typical photocurrent density versus photovoltage characteristics (power output characteristics) of $n$-$CdSe_{0.6}Te_{0.4}$ film /polysulphide under illumination of 100 mW/cm$^2$ intensity are shown in Fig. 8. The efficiency, $\eta$ (in %) was calculated from the relation

$$\eta = \frac{V_{OC} J_{SC} \mathrm{FF} 100}{P}, \tag{8}$$

where $P$ is the input light intensity. The Fill factor (FF) was calculated from the relation

$$\mathrm{FF} = \frac{V_m J_m}{V_{OC} J_{SC}}. \tag{9}$$

Series resistance $R_s$ and shunt resistance $R_{sh}$ were evaluated from the slopes of the power output characteristics using the relations (Coutts[26])

$$\left(\frac{dI}{dV}\right)_{I=0} \approx \frac{1}{R_s}, \tag{10}$$

$$\left(\frac{dI}{dV}\right)_{V=0} \approx \frac{1}{R_{sh}}. \tag{11}$$

Important parameters that are obtained from the power output plots are tabulated in Table II.

TABLE II. Important parameters obtained from power output plots.

| Sl no. | Condition of the thin film | $J_{SC}$ ($\mu$A/cm$^2$) | $V_{OC}$ (mV) | FF (%) | $\eta$ (%) | $R_s$ ($\Omega$) | $R_{sh}$ ($\Omega$) |
|---|---|---|---|---|---|---|---|
| 1 | unnealed, unetched | 6800 | 560 | 40 | 1.53 | 100 | 250 |
| 2 | unannealed, etched | 7500 | 580 | 44 | 1.93 | 18.2 | 1000 |
| 3 | annealed unetched | 8900 | 600 | 50 | 2.72 | 18.1 | 2000 |
| 4 | annealed, PEC etched | 10 000 | 650 | 59 | 3.83 | 18 | 1804 |

It can be seen from Table II that the shunt resistance also changes favorably on surface treatment. The etched film shows an improvement from 250 to 1000 $\Omega$. The unetched but annealed film shows an increase of from 250 to 2000 $\Omega$, however, on photoelectrochemically etching the annealed film a change of shunt resistance from 250 to 1804 $\Omega$ could be achieved.

Shunt resistance $R_{sh}$ in the case of the thin-film polycrystalline solar cell mainly arises due to the columnar grains with lengths close to the thickness of the thin film itself. For thin films with low packing density of grains, there is a likelihood of easy leakage paths through the grain boundaries. The process of annealing increases the packing density and strong adhesion to the substrate. Etching and photoelectrochemical etching processes contribute to the increase in the junction area so that an increase in the shunt resistance is observed. For an ideal solar cell, shunt resistance should be infinite.

It is also seen that the series resistance $R_s$ also changes to favorably better values on surface treatment. From Table I it is seen that the series resistance $R_s$ decreases appreciably for an unannealed film from 100 to 18.1 $\Omega$ (on annealing) and on etching the film it decreases from 100 to 18 $\Omega$. There is no drastic change in the reduction of series resistance $R_s$ on further photoelectrochemical etching as most of the contribution to the series resistance comes from the contacts to the thin film and the external circuit. The larger the contact area, the smaller will be the series resistance.

It is seen from Table I that on chemical etching the open circuit voltage and the short-circuit current density increase. Etching also removes the few oxide layers which are present *ab initio* during the film formation. It also removes the surface states and dislocations, thus leading to an improvement in the efficiency and stability[27] of the thin film electrode in the polysulphide electrolyte.

The main effect of photoelectrochemical etching is the formation of etch pits which increases the area of the junction by nearly 50%. This increase in the area reduces the reflectivity of the surface by nearly 10% so that the interaction of holes with the electrolyte is considerably improved. Photoelectrochemical etching also increases the surface roughness of the electrode and has the effect of reducing the effective surface concentration of holes per unit area of the junction. Thus, only a limited number of (sufficiently adequate) holes is available to interact with the sulphide species, thus nullifying the problem of photocorrosion if the holes had been present in excess.

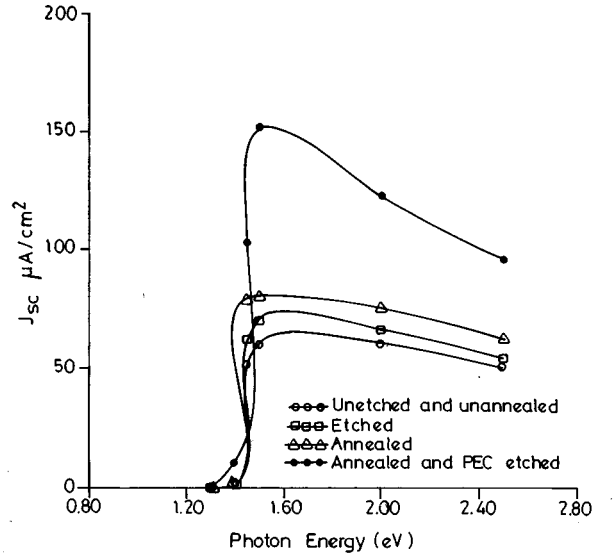


FIG. 9. A plot of $J_{sc}$ as function of photon energy for $n$-$CdSe_{0.6}Te_{0.4}$/polysulphide PEC solar cell under various conditions.

### 4. Spectral response studies

Spectral response studies were conducted for an $n$-$CdSe_{0.6}Te_{0.4}$ thin film/polysulphide PEC system by plotting the short-circuit photocurrent density ($J_{SC}$) as a function of photon energy (eV). It is seen from Fig. 9 that at the onset of photon energy at the edge of the band gap there is a sharp rise in the photocurrent density for the annealed and PEC etched film, attaining a maximum. The fall in the short-circuit current density at the higher side of the photon energy is due to the fact that the polysulphide electrolyte exhibits strong absorption of light.[28]

Quantum efficiency is defined by the equation[29]

$$Q_F = \frac{\text{no. of photoelectrons generated/area}}{\text{no. of incident photons/area}}, \tag{12}$$

and is calculated from the equation:

$$Q_F = \frac{J_{SC}(\text{A/cm}^2)h\nu(\text{eV})}{q \text{ intensity of light (W/cm}^2)}. \tag{13}$$

As per Butler,[24]

$$Q_F = 1 - \frac{\exp(-\alpha\omega)}{1+\alpha L_p}, \tag{14}$$

where $L_p$ is the diffusion length of holes, $\omega$ is the depletion width, and $\alpha$ is the absorption coefficient. A plot of quantum efficiency as a function of photon energy (eV) in Fig. 10 indicates that the PEC etched photoelectrodes yield a maximum yield of about 82% which is also confirmed from the power output characteristics. The as-grown, unannealed, and unetched film gives a low yield of 38% due to lack of texture and small grains as evidenced from the SEM photomicrographs. However, the etched and annealed film gives a better

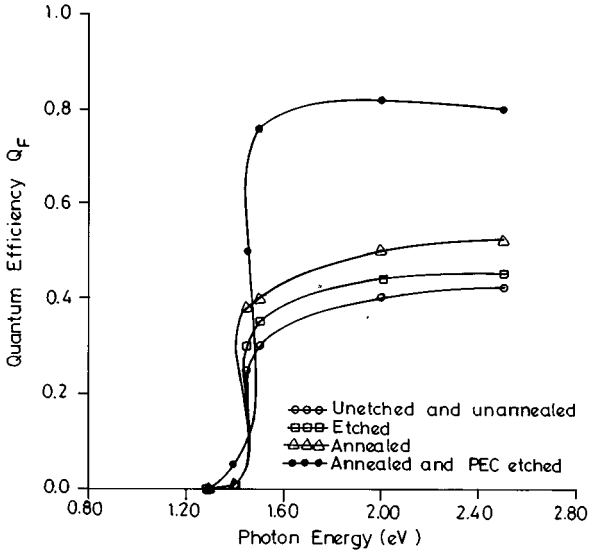


FIG. 10. A plot of quantum efficiency as function of photon energy for $n$-$CdSe_{0.6}Te_{0.4}$/polysulphide PEC solar cell.

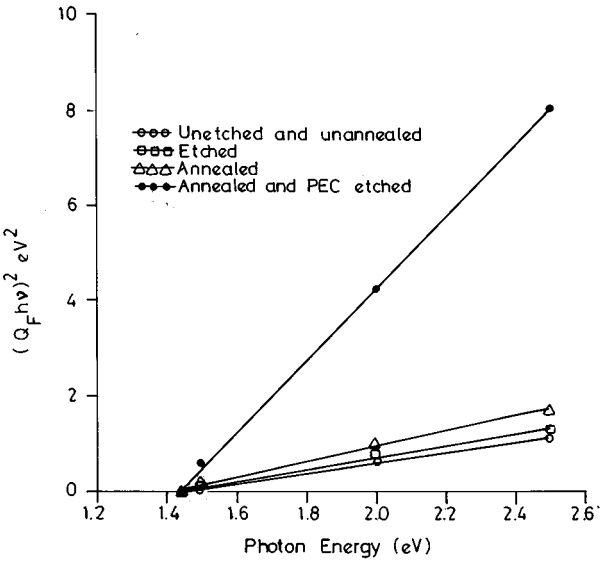


FIG. 11. A plot of $(Q_F h\nu)^2$ as a function of photon energy for $n$-$CdSe_{0.6}Te_{0.4}$/polysulphide PEC solar cell.

yield of about 50% due to an increase in texture and grain size and a decrease in grain density leading to lesser scattering.

In the vicinity of the absorption edge, such that $\alpha L_p \ll 1$ and $\alpha\omega \ll 1$ expanding Eq. (13) and neglecting the higher powers of the series expansion of $\exp(-\alpha\omega)$, we get

$$Q_F \approx \alpha(\omega + L_p). \tag{15}$$

Substituting the expression for $\alpha$ from Eq. (1) in Eq. (14) we get

$$Q_F \approx \frac{A^*}{h\nu}(h\nu - E_g)^{1/2}(\omega + Lp). \tag{16}$$

Therefore,

$$(Q_F h\nu)^2 \approx A^{*2}(h\nu - Eg)(\omega + L_p)^2. \tag{17}$$

The experimental plot of $(Q_F h\nu)^2$ vs $h\nu$ is linear, as shown in Fig. 11 as expected from the above equation. The intercept on the energy axis gives the band gap energy,[27] $E_g \approx 1.45$ eV. This value is quite close to the value obtained from the optical absorption measurements using Eq. (1).

A plot of quantum efficiency vs applied potential in Fig. 12 indicates that the quantum efficiency $Q_F$ remains fairly constant for potentials more positive than $-500$ mV versus SCE indicating that Gärtner's model can be applied in this range.[30]

It has been shown by several authors[31,32] that Gärtner's model of metal–semiconductor provides a successful description of semiconductor-electrolyte junction.

As per Kennedy,[31] the photocurrent is given by

$$I_{ph} = -q\phi_0[1 - (e^{-\alpha\omega})]/(1 + \alpha L_p), \tag{18}$$

where $\omega$, is the depletion width in the semiconductor. As per Gärtner[32] the quantum efficiency $Q_F$ the minority carrier hole diffusion length $L_p$, and the depletion width $\omega$ are related by

$$\ln(1 - Q_F) = -\alpha\omega_0(V - V_{FB})^{1/2} - \ln(1 + \alpha L_p). \tag{19}$$

Hence, a plot of $\ln(1-Q_F)$ vs $(V - V_{FB})^{1/2}$ should be linear. The experimental plot of $\ln(1-Q_F)$ vs $(V - V_{FB})^{1/2}$ drawn in our case is linear (Fig. 13) as is expected. The slope of the plot gives the donor concentration and the intercept on the vertical axis gives the minority carrier diffusion length. It is seen that the donor concentration decreases with annealing and etching treatments from $6.24\times10^{16}$ to $1.27\times10^{16}$ $cm^{-3}$. The corresponding minority carrier diffusion length increases from $2.97\times10^{-6}$ to $4.73\times10^{-6}$ cm. This is clearly reflected in the power output characteristics and the $I_{ph}^2$ versus applied potential plot (Fig. 7).

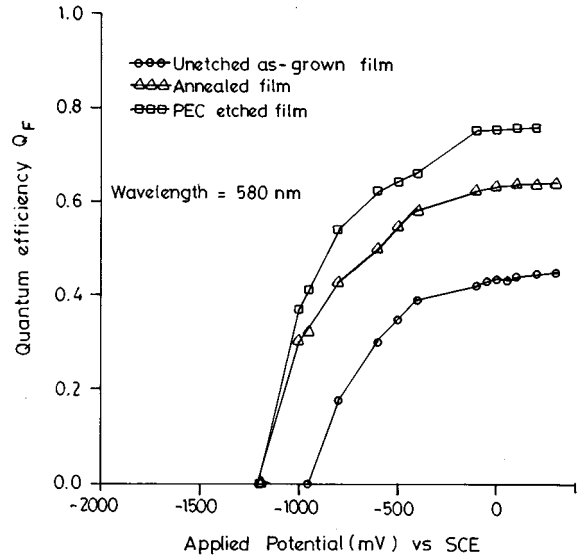


FIG. 12. A plot of quantum efficiency as function of applied potential for different surface treatments of $n$-$CdSe_{0.6}Te_{0.4}$/polysulphide PEC solar cell.

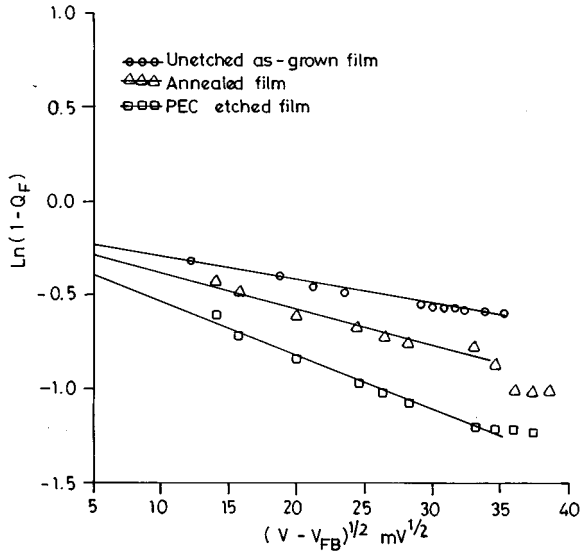


FIG. 13. A plot of $\ln(1-Q_F)$ as a function of $(V-V_{FB})^{1/2}$ using the Gärtner model.

## IV. CONCLUSIONS

Annealing of the thin-film photoanode helps in improving and increasing the grain size considerably and thus enhancing the efficiency of the photoelectrochemical solar cells from 1.53% to 2.72% and fill factor from 40% to 50%. Etching improves the efficiency of PEC cells from 1.53% to 1.93% and fill factor from 40% to 44%. On photoelectrochemical etching, efficiency improves remarkably from 1.53% to 3.83%. It also improves the surface roughness, texture, and stability, and inhibits photocorrosion of the semiconducting thin film electrode.

## ACKNOWLEDGMENT

The authors thank D. Shanthi, Department of Metallurgy, for taking the scanning electron micrographs and Dr. M. V. Sangaranarayanan, Department of Chemistry for useful discussions.

[1] H. Gerisher, Electrochim. Acta **35**, 1677 (1990).
[2] H. Gerisher, Electrochim. Acta **58**, 263 (1975).
[3] M. A. Russak and C. Crater, J. Electrochem. Soc. **13**, 556 (1984).
[4] L. Clement, R. Triboulet, J. Rioux, and A. Etchberry, J. Appl. Phys. **58**, 4703 (1985).
[5] V. Damodara Das, Sahil Kirupavathy, and L. Damodare, and N. Lakshminarayan, J. Appl. Phys. **79**, 8521 (1996).
[6] M. Bouroushian, Z. Loizos, N. Spyrellis, and G. Maurin, Thin Solid Films **229**, 101 (1993).
[7] M. Skyllas-Kazacos, J. Electroanal. Chem. **148**, 233 (1983).
[8] P. J. Sebastian, Ph.D. thesis, Indian Institute of Technology, Madras, India, 1990.
[9] V. Damodara Das and L. Damodare, Solid State Commun. **99**, 723 (1996).
[10] J. I. Pankove, in *Optical Processes in Semiconductors*, Solid State Physical Electronics Series, edited by N. Holonyak, Jr. (Prentice–Hall, Englewood Cliffs, NJ, 1971), p. 34.
[11] M.T Gutterriez, Sol. Energy Mater. Sol. Cells **21**, 283 (1991).
[12] N. F. Mott, Proc. R. Soc. London Ser. A **171**, 27 (1939).
[13] W. Schottky, Z. Phys. **113**, 367 (1939).
[14] Y. Wada and S. Nishimatsu, J. Electrochem. Soc. **125**, 1499 (1978).
[15] F.C. Hull and W. J. Howk, J. Met. **5**, 565 (1953).
[16] V. Damodara Das and L. Damodare, Semicond. Sci. Technol. (to be published).
[17] P. Herrasti, E. Fatas, J. Herrero, and J. Ortega, Electrochim. Acta **35**, 345 (1990).
[18] W. H. Laflere, F. Cardon, and W. P. Gomes, Surf. Sci. **44**, 541 (1974).
[19] W. H. Laflere, R. L. Van Meirhaeghe, and F. Cardon, Surf. Sci. **59**, 541 (1976).
[20] *Semiconductor Electrodes, Studies in Physical and Theoretical Chemistry*, edited by H. O. Finklea (Elsevier, Amsterdam, 1988), Vol. 55.
[21] R. A. L. Van der Berghe, F. Cardon, and W. P. Gomes, Surf. Sci. **39**, 368 (1973).
[22] H. Gerisher, in *Photovoltaic and Photoelectrochemical Solar Energy Conversion*, edited by F. Cardon and W. P. Gomes (Plenum, New York, 1981), p. 199.
[23] J. A. Turner, J. Chem. Ed. **60**, 327 (1983).
[24] M. A. Butler, J. Appl. Phys. **48**, 1914 (1977).
[25] N. S. Lewis and M. L. Rosenbluth, in *Photocatalysis, Fundamentals and Applications*, edited by N. Serpone and E. Pellizetti (Wiley, New York, 1989).
[26] T. J. Coutts, Sol. Energy Mater. **50**, 99 (1978).
[27] R. Tenne and N. Muller, J. Electrochem. Soc. **130**, 852 (1983).
[28] Z. Deng, M. Cinquino, and M. F. Lawrence, J. Mater. Res. **6**, 1293 (1991).
[29] S. Chandra and R. K. Pandey, Phys. Status Solidi A **1**, 1 (1982).
[30] M. T. Gutierrez and J. Ortega, Sol. Energy Mater. **20**, 387 (1990).
[31] J. H. Kennedy and K. W. Frese, Jr., J. Electrochem. Soc. **123**, 1683 (1976).
[32] W. W. Gärtner, Phys. Rev. **116**, 84 (1959).